Wear 546–547 (2024) 205332

Contents lists available at ScienceDirect

Wear

journal homepage: www.elsevier.com/locate/wear

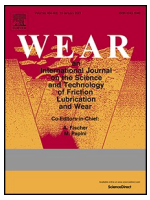

Emission and properties of airborne wear particles from train brake friction materials based on novolac phenolic resins and butadiene rubbers

Yurii Tsybrii [a,*], Oleksii Nosko [a], Izabela Zglobicka [b], Michal Kuciej [b]

[a] Gdansk University of Technology, Faculty of Mechanical Engineering and Ship Technology, ul. G. Narutowicza 11/12, Gdansk, 80-233, Poland
[b] Bialystok University of Technology, Faculty of Mechanical Engineering, ul. Wiejska 45C, Bialystok, 15-351, Poland

ARTICLE INFO

Keywords:
Brakes
Fillers
Wear
Particles

ABSTRACT

The emission of airborne particulate matter from a train brake depends on the formulation of its friction material. This study investigates the emission and properties of wear particles from train brake friction materials based on straight or resorcinol-modified novolac phenolic resin and nitrile or styrene butadiene rubber used as binding ingredients. The wear particles are generated by a pin-on-disc tribomachine inside an aerodynamic chamber, counted and collected using aerosol measurement techniques, subjected to microscopic and elemental analysis. It has been found that the modification of novolac phenolic resin with resorcinol has no considerable effects on the emission of wear particles and their properties. By contrast, replacing styrene butadiene rubber with nitrile butadiene rubber leads to a significant decrease in the emission of 0.1–10 μm wear particles.

1. Introduction

Airborne wear particle emission from transport vehicles constituted essential research topic since the beginning of the 21st century. Passenger cars are considered as the main contributor of wear particulate matter because of their quantitative predominance (Kukutschová and Filip [1], Adamiec [2]). On the other hand, frequent operation of transport vehicles in a closed or semi-closed area, such as traffic of trains in an underground station, leads to the accumulation of wear particles in the air within this area (Cheng et al. [3], Fridell et al. [4], Gustafsson et al. [5]). Their concentration depends on many factors including the underground station configuration, its proximity to the outside environment, air conditioning system and traffic intensity (Abbasi et al. [6], Colombi et al. [7], Cartenì et al. [8], Cusack et al. [9], Cha et al. [10]). The main sources of train-related wear particles are wheel–rail contacts (Lee [11]) and mechanical brakes (Olofsson [12], Namgung et al. [13], Tsybrii et al. [14], De Falco et al. [15]). The particles emitted from a wheel–rail steel contact contain heavy metals and their oxides, whilst the particles originating from wearing a multi-ingredient brake material against a steel surface may additionally contain phenol formaldehyde resins (PF), rubbers and the products of their chemical reactions (Kukutschová et al. [16], Jara and Jang [17], Nogueira et al. [18]). When the wear particles are inhaled, they carry the toxic substances mentioned above into the human body, leading to respiratory, cardiovascular, allergic and cancerous diseases (Pope et al. [19], Karlsson et al. [20], Bigert et al. [21]). Therefore, many international programs and initiatives involving academic institutions and industrial research centres aim at finding ways to reduce wear particle emissions from trains with a particular focus on brake emissions.

Traditionally, the ingredients used to produce friction materials (FM) for brakes are classified in four categories: binders, fillers, reinforcements and friction modifiers (Borawski [22]), although some of the ingredients may perform more than one function (Jeganmohan et al. [23]). One of the most popular binders is PF with content in range 5–35 wt% (Binda et al. [24]) because of its low cost, good mechanical properties, chemical and thermal resistivity, as well as stable tribological properties (Tang et al. [25], Liu et al. [26], Menapace et al. [27], Fareez et al. [28]). PF and, specifically, novolac PF (NPF) are commonly used as binding ingredients for FM of train brakes (Shojaei et al. [29], Wasilewski [30], Sawczuk et al. [31]).

The tribological properties of FM based on PF are affected substantially by its content, molecular weight and modification. Nogueira et al. [18] reported that an increase in the PF content results in a decrease in the coefficient of friction (COF). Jara and Jang [17] and Joo et al. [32] showed that FM with higher molecular weight PF exhibit improved friction and wear characteristics. PF can be modified using physical or chemical approach. The physical approach, which relies on blending modifiers, is not very common due to a small influence it exerts on the

* Corresponding author.
E-mail address: yurii.tsybrii@pg.edu.pl (Y. Tsybrii).

https://doi.org/10.1016/j.wear.2024.205332
Received 9 October 2023; Received in revised form 28 February 2024; Accepted 7 March 2024
Available online 13 March 2024

molecular structure of PF (Gooch [33]). By contrast, the chemical approach yields changes in the PF molecular structure and, accordingly, allows obtaining FM with improved properties (Ge et al. [34]). When developing a new FM, attention is paid to those modifications that improve the thermal resistivity (e.g. polyamide, amine, molybdenum, phosphorous, epoxy, vegetable oil), mechanical strength (e.g. polyamide, maleimide, dicyandiamide) and wear resistance (e.g. polyamide, amine). Motawie and Sadek [35] reported that the modification of PF with resorcinol allows improving its shear strength and coating properties. Note that not so many modified PF are used by FM manufacturers due to high costs of their production, whilst straight PF remains the predominant binder (Gurunath and Bijwe [36]).

The role of fillers in FM consists in filling up the space between other ingredients. There are various fillers like rubber, vermiculite, perlite, barium sulphate and cellulose (Borawski [22]). Among the rubbers used as filling and binding ingredients for FM of train brakes, nitrile butadiene rubber (NBR) and styrene butadiene rubber (SBR) should be mentioned (Shojaei et al. [29], Wasilewski [30]). Added in their powdered form, NBR and SBR enable improving the mechanical, vibrational, chemical and tribological properties of FM (Akshay et al. [37], Liu et al. [38]). Surojo et al. [39] found that an increase in the NBR content leads to higher elastic modulus and flexural strength and a lower wear rate, which is explained by the capability of NBR to strengthen the adhesion between the FM matrix and other ingredients (N. Bijwe and J. Bijwe [40]). On the other hand, Tamayo et al. [41] and Saffar and Shojaei [42] found that the addition of SBR to FM results in a reduction in the mechanical properties and wear resistance yet an increase in COF. Furthermore, the addition of 2.5 wt% NBR and 2.5 wt% SBR improves the frictional behaviour in brake fade (Jeganmohan et al. [23]). NBR and SBR are also added in the form of nanopowders, which allows improving the tribological properties even to a greater extent (Liu et al. [38]). It should be noted that excessive content of rubber in FM may have negative effects, too. For example, Mutlu et al. [43] reported an increase in the wear rate for FM containing 15 wt% of waste tyre dust.

Despite a large number of studies investigating the influence of PF and rubber ingredients on the mechanical, thermal and tribological behaviour of FM, studies devoted to the effects of PF and rubber ingredients on the emission of wear particles are still scarce. Nogueira et al. [18] mentioned that the influence of the PF content on the wear particle emission is complicated since its increase leads to a higher mechanical integrity of FM and simultaneously a larger contact area. Joo et al. [44] investigated the wear particle emission from FM based on PF and its modifications at elevated temperatures. Their experiments showed that the modification of PF with aromatic ring, silicon or acryl leads to a reduction in the emission of particles below 2.5 μm, whereas alkyl-modified PF exhibits a more intensive particle emission compared to straight PF. Song et al. [45] investigated the influence of PF curing conditions on the brake particle emission. An artificial neural network intended for optimising the curing conditions was developed. There are, however, no previously obtained experimental data available on the particle emission effects of NPF and resorcinol-modified NPF (RNPF).

The present study investigates the concentration, size distribution, morphology and elemental composition of airborne wear particles emitted from train brake FM based on NPF or RNPF and NBR or SBR binders in relation to the mechanical properties of FM and wear mechanism.

2. Experimental

2.1. Friction materials

Three experimental FM were produced in the form of brake linings by a multistage technological process intended for production of train brake linings. The technological process includes dry mixing of the ingredients, seasoning and milling of the mixture, hot moulding and curing. Pin samples of 8 mm diameter and 8 mm height were milled out from the brake linings by a 6040T4D milling machine. Their friction surfaces remained unaltered during the milling. Disc samples measuring 60 mm in diameter and 6.5 mm in thickness were S235JR steel. The roughness of the friction surfaces of the disc samples was Ra 2.5.

The formulations of FM are shown in Table 1. The first FM denoted as $M_{RNPF/NBR}$ contains 11.2 wt% RNPF and 11.2 wt% NBR binders. The second FM denoted as $M_{NPF/NBR}$ differs from $M_{RNPF/NBR}$ by the replacement of RNPF with NPF. In the third FM denoted as $M_{RNPF/SBR}$, SBR is used instead of NBR. The other ingredients in the studied FM are identical and include steel fibre, graphite, mineral fibre, calcium carbonate, stibnite, vulcaniser and hardening agent. Note that the formulations of FM are similar to those used for commercial linings of train brakes.

The original friction surfaces of the pin and disc samples were analysed using scanning electron microscopy (SEM) and energy dispersive X-ray spectroscopy (EDX). Table 2 presents the averaged elemental compositions of the friction samples, whilst Fig. 1 shows the EDX maps of the original friction surface of an exemplary pin sample. Comparison of Table 1, Table 2 and Fig. 1 for the pin samples suggests that iron originates from the steel fibre; silicon, aluminium and magnesium originate from the mineral fibre; and calcium originates from the calcium carbonate powder.

Table 3 presents the mechanical properties of FM including the density, elastic modulus (UIC 541-4), compression strength (PN-EN ISO 604:2006), shear strength (PN-92/S-47041), bending strength (PN-EN ISO 178:2006) and HRX hardness (UIC 541-4). According to the presented data, $M_{NPF/NBR}$ and $M_{RNPF/SBR}$ exhibit similar mechanical properties, whereas $M_{RNPF/NBR}$ is characterised by higher hardness and strength.

2.2. Pin-on-disc tribomachine

The present study was conducted using an experimental set-up built on the basis of a T-11 pin-on-disc tribomachine, as shown in Fig. 2. A dead weight pressed the pin sample against the disc sample. The disc sample was mounted on a disc sample support. The friction radius was 20 mm. The friction force was measured by an HBM S2 sensor with the resolution of 0.01 N. COF μ was calculated as the ratio of the measured friction force to the known load on the pin sample. The temperature T of the pin sample was measured by a K-type thermocouple. The thermocouple was installed in a 0.6 mm diameter blind hole parallel to the pin sample axis. The initial distance between the thermocouple measuring junction and friction surface was 1 mm. The thermocouple signal was sampled by a Graphtec GL7000/GL7-HSV data logger with 1 Hz frequency and 0.01 °C resolution. The mass wear w_{disc} and w_{pin} of the respective disc and pin samples was measured by a Radwag XA 210.4Y.A analytical balance with the resolution of 10^{-5} g.

2.3. Airborne wear particle measurement system

The studied friction pair was isolated from the environment by an

Table 1
Friction material formulation, wt%.

Ingredient	Friction material		
	$M_{RNPF/NBR}$	$M_{NPF/NBR}$	$M_{RNPF/SBR}$
Resorcinol-modified novolac phenol formaldehyde (RNPF)	11.2		11.2
Novolac phenol formaldehyde (NPF)		11.2	
Nitrile butadiene rubber (NBR)	11.2	11.2	
Styrene butadiene rubber (SBR)			11.2
Steel fibre	30	30	30
Graphite	16.1	16.1	16.1
Mineral fibre	14.7	14.7	14.7
Calcium carbonate	12.6	12.6	12.6
Stibnite	3.2	3.2	3.2
Vulcaniser and hardening agent	1	1	1

Table 2
Elemental compositions of the friction samples, wt%.

Element	Pin sample			Disc sample
	$M_{RNPF/NBR}$	$M_{NPF/NBR}$	$M_{RNPF/SBR}$	
C	45.8	41.6	45.3	0.17
O	16	8.64	11.7	
Mg	0.5	0.29	0.32	
Al	1.4	0.97	1.09	
Si	2.75	1.83	1.93	0.6
S	2.8	2.68	2.75	
Ca	10.7	8.74	9.29	
Mn				1.4
Fe	20.1	35.3	27.7	97.2
Cu				0.55

Table 3
Mechanical properties of the friction materials.

Property	Pin sample			Disc sample
	$M_{RNPF/NBR}$	$M_{NPF/NBR}$	$M_{RNPF/SBR}$	
Density, g/cm^3	2.4	2.3	2.4	7.8
Elastic modulus, GPa	1.3	1.0	1.1	
Compression strength, MPa	61	41	40	
Shear strength, MPa	15	13	11	
Bending strength, MPa	22	19	19	
Hardness	77 HRX	62 HRX	66 HRX	124 HB

aerodynamic chamber. The volume inside the aerodynamic chamber was 0.55 L. The room air was supplied by a Bambi PT50D compressor through a 50 L receiver and a TSI Filtered Air Supply 3074B filter to the aerodynamic chamber inlet. The inlet airflow was adjusted at 12 L/min using an RFL-B-3/8 needle valve and a TSI Flow Calibrator 4048. Wear particles emitted from the friction contact were transported by the airflow inside the aerodynamic chamber to its outlet. The air coming from the outlet was sampled and analysed by TSI Optical Particle Sizer 3330 (OPS), TSI NanoScan SMPS Nanoparticle Sizer 3910 (SMPS) and Dekati PM10 Cascade Impactor (CI) with respective airflow rates 1, 0.75 and 9.75 L/min.

OPS counts aerosol particles with optical diameter 0.3–10 μm and classifies them into 16 groups at 1 Hz frequency. SMPS counts 0.01–0.42 μm aerosol particles based on the electric mobility and performs their classification into 13 groups at the frequency of one particle

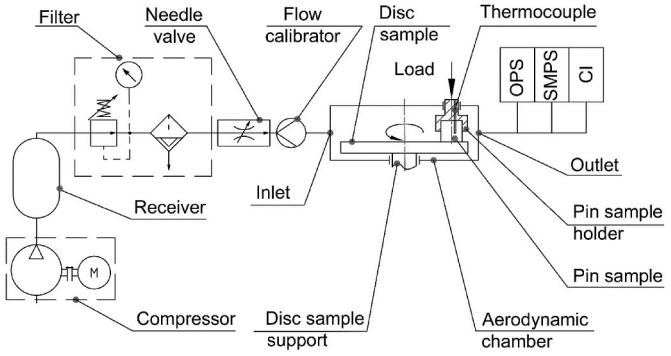

Fig. 2. Experimental set-up.

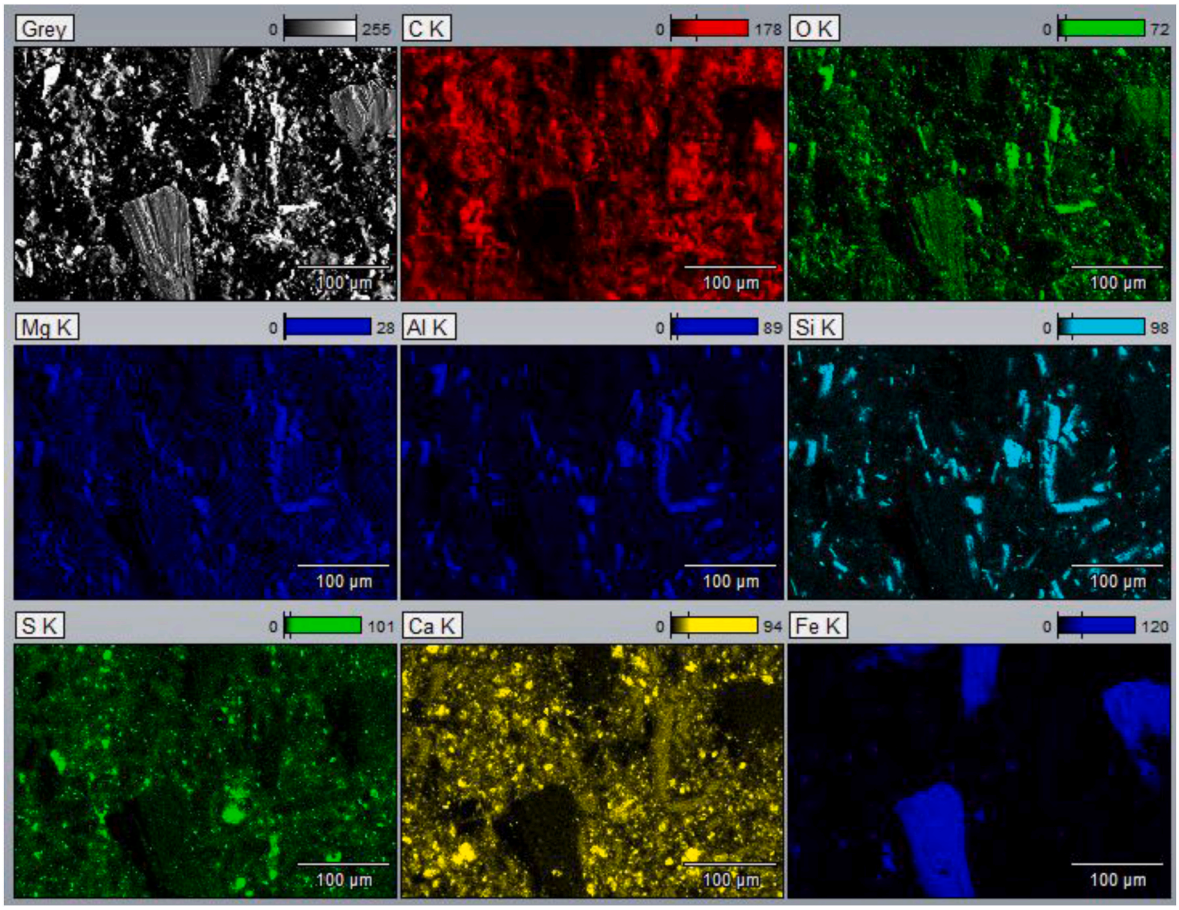

Fig. 1. EDX maps of the original friction surface of the pin sample $M_{RNPF/NBR}$.

size distribution per minute. The particle concentrations in no/cm^3 measured by OPS and SMPS are denoted by C_{OPS} and C_{SMPS}, respectively. CI collects aerosol particles with aerodynamic diameter ranges >10 μm, 2.5–10 μm and 1–2.5 μm on aluminium foils for further SEM/EDX analysis.

2.4. SEM/EDX analysis of the friction samples and collected wear particles

SEM analysis was performed using an ultra-high-resolution analytical system Thermo Scientific Scios 2 Dual Beam FIB-SEM with acceleration voltage 2 kV and magnification up to 30000×. EDX analysis was conducted using a NORAN System 7 energy dispersive full range X-ray microanalysis system with 20 kV voltage and 10 kV elemental range.

2.5. Friction conditions

Before starting the test, the aerodynamic chamber, components of the tribomachine inside the aerodynamic chamber, connection tubes and CI components were carefully cleaned. New pin and disc samples were air-blown, SEM/EDX analysed, weighed and installed in the tribomachine. New foils were installed in CI. The tribomachine, data logger, analytical balance, OPS and SMPS were systematically calibrated. The filter efficiency was ensured by checking that C_{OPS} equals zero and C_{SMPS} is below 100 no/cm^3 (noise level) in the absence of friction. After the test, the worn friction samples were carefully dismantled, air-blown and weighed. The worn friction samples and CI foils were then subjected to SEM/EDX analysis. The influence of uncontrolled factors was minimised by performing the experimental procedures in a similar manner by the same operator.

There were six friction regimes (FR) differing in the contact pressure (0.66, 1 MPa) and sliding speed at the friction radius (0.6, 1.2, 1.8 m/s). Three tests were carried out in each FR to estimate the test-retest repeatability. The test duration was 2 h. The environment temperature was 22 ± 2 °C and the relative humidity was 35 ± 5%.

The typical results obtained during a single test are shown in Fig. 3. During the first hour of the test, a running-in of the friction pair occurred with unpredictable changes in COF μ and particle concentrations C_{OPS} and C_{SMPS} and increasing pin sample temperature T. The frictional behaviour stabilised gradually, and it was almost steady for the second hour of the test. Accordingly, the measured quantities μ, T, C_{OPS} and C_{SMPS} were averaged over the second hour of the test to be characteristic.

It is important to mention that the contact pressure in 1 MPa order is typical for train brakes and comparable to the values used in a Kraus-type machine study by Joo et al. [44] and a full-scale dynamometer study by Saffar and Shojaei [42]. As regards the sliding speed, its maximum value of 1.8 m/s limited by the tribomachine characteristics is substantially lower than those in a train brake and corresponds to the lowest value used in a sub-scale dynamometer study by Wang et al. [46]. Thereby, FR of the present study simulate very mild speed and temperature conditions.

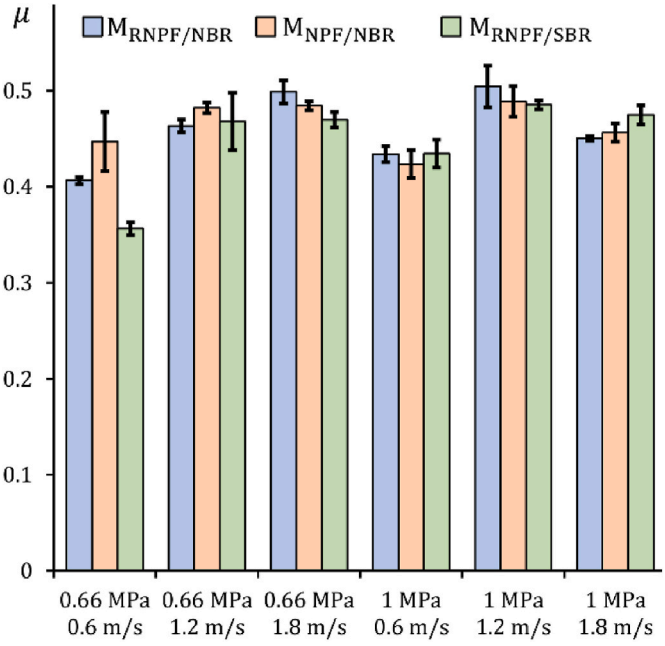

Fig. 4. Coefficient of friction μ depending on the friction regime.

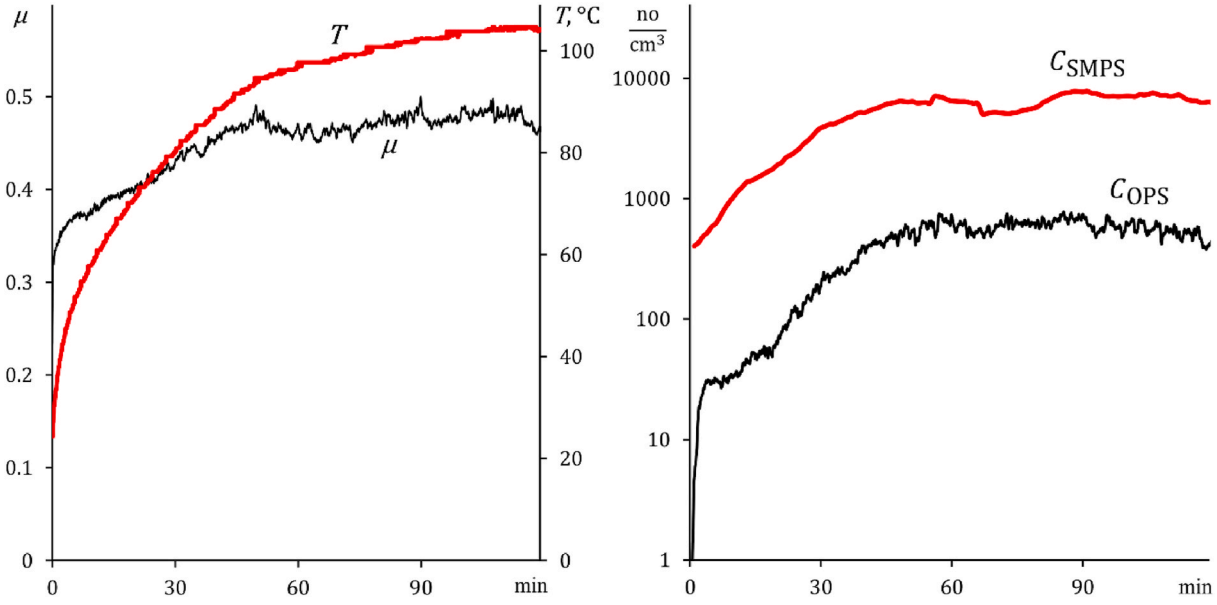

Fig. 3. Typical results of a single test ($M_{NPF/NBR}$, 1 MPa × 1.2 m/s).

3. Results

3.1. Friction and wear

Fig. 4 shows the measured COF μ. The bars show average values, whilst the line segments indicate ± standard deviation intervals. It is seen that the entire range of variation of μ is 0.35–0.5. FM exhibit similar values of μ in all FR, except for the mildest FR of 0.66 MPa × 0.6 m/s. Here, replacing NBR with SBR, i.e. $M_{RNPF/NBR} \rightarrow M_{RNPF/SBR}$, results in smaller μ.

Fig. 5 shows the measured pin sample temperature T. As presented, T is about 50 °C in the mildest FR of 0.66 MPa × 0.6 m/s, whilst it reaches a value of about 160 °C in the heaviest FR of 1 MPa × 1.8 m/s. Thereby, T does not exceed 160 °C in all FR. Noticeably, the pin sample $M_{RNPF/SBR}$ is heated to a higher temperature compared to the other FM, except for the mildest FR of 0.66 MPa × 0.6 m/s, which correlates with the smaller value of μ for this FR, as mentioned above.

Fig. 6 presents the measured mass wear w_{disc} and w_{pin} of the respective disc and pin samples. In general, w_{disc} and w_{pin} become larger with increasing contact pressure or sliding speed. It can be seen that the pin sample wear w_{pin} increases as NBR is replaced with SBR, i.e. $M_{RNPF/NBR} \rightarrow M_{RNPF/SBR}$. The disc sample wear w_{disc} decreases with $M_{RNPF/NBR} \rightarrow M_{NPF/NBR}$ or $M_{RNPF/NBR} \rightarrow M_{RNPF/SBR}$ in the heavier FR, except for the heaviest one of 1 MPa × 1.8 m/s where the scatter in the measured values is too large to draw a specific conclusion.

3.2. Worn surfaces

Fig. 7 shows the SEM images of the worn surfaces of the pin and disc samples. Primary plateaus of 100 μm order size can be distinguished on the worn surfaces of the pin samples. These plateaus are covered with numerous ploughing grooves. The worn surface of the disc sample is also covered with ploughing grooves, as shown on the example of the disc sample in pair with the pin sample $M_{NPF/NBR}$.

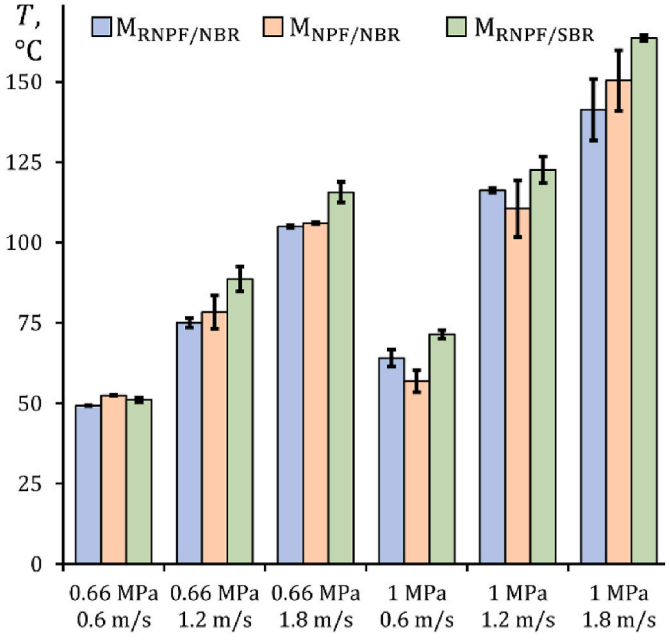

Fig. 5. Pin sample temperature T depending on the friction regime.

Fig. 8 shows the EDX maps of the worn surface of an exemplary pin sample $M_{RNPF/SBR}$. EDX analysis reveals a significant content of iron in the primary plateaus. Additionally, the mineral fibre in the form of silicon, aluminium, magnesium and oxygen elements and the calcium carbonate powder can be identified.

3.3. Emission of airborne wear particles

Fig. 9 illustrates the measured particle concentrations C_{OPS} and C_{SMPS} in logarithmic scale. The order of magnitude of C_{OPS} varies between 10 no/cm^3 in the milder FR and 10^3 no/cm^3 in the heavier ones. The diagram of C_{SMPS} is qualitatively consistent with that of C_{OPS}. It can be seen that replacing NBR with SBR, i.e. $M_{RNPF/NBR} \rightarrow M_{RNPF/SBR}$, leads to an increase in both C_{OPS} and C_{SMPS}. On the other hand, no distinct trend is observed in response to the change $M_{RNPF/NBR} \rightarrow M_{NPF/NBR}$. Note that due to the measurement sensitivity of SMPS, the concentration data below 10^2 no/cm^3 are not reliable.

Merging the measurements from OPS and SMPS allows finding the particle size distribution in size range 0.01–10 μm. Fig. 10 shows the OPS and SMPS distributions obtained for the studied FM, eliminating the SMPS concentrations below 10^2 no/cm^3. It is shown that the fine wear particles (0.1–2.5 μm) predominate with a distinct global peak at 0.15 μm indicated by SMPS and two local peaks at 0.5 and 1.6 μm indicated by OPS. The replacement of NBR with SBR, i.e. $M_{RNPF/NBR} \rightarrow M_{RNPF/SBR}$, results in higher particle concentrations in size range 0.1–10 μm, which is in line with Fig. 9.

3.4. Properties of airborne wear particles

Fig. 11 shows the SEM images of the CI foils with collected wear particles. Particles of various shape and size ranging between 0.1 and 10 μm are present. Larger particles of 1–10 μm size have normally flaky shape. Further, primary particles of submicron size are more rounded. Moreover, particle agglomerations are frequently met in the form of combination of comparable size particles or combination of a larger particle and attached smaller ones. No qualitative differences in the particles originated from different FM have been revealed.

Fig. 12 shows two exemplary EDX maps of the collected wear particles. These maps allow identifying 1–10 μm particles composed mainly of iron. Further, Fig. 12a shows several 1–5 μm particles with noticeable content of calcium. Furthermore, Fig. 12b indicates two particles containing silicon, aluminium, magnesium and oxygen, whose size is approximately 5 μm.

4. Discussion

The experimental data (see Fig. 4) show no considerable difference in COF for the studied FM, although the variation ranges for the contact pressure and sliding speed are narrow in the present study. Some interesting relations can, however, be obtained for the wear characteristics (see Fig. 6). Fig. 13 shows the values of the relative wear of the disc sample calculated as $w_{disc}/(w_{disc} + w_{pin})$. There is a decrease in the

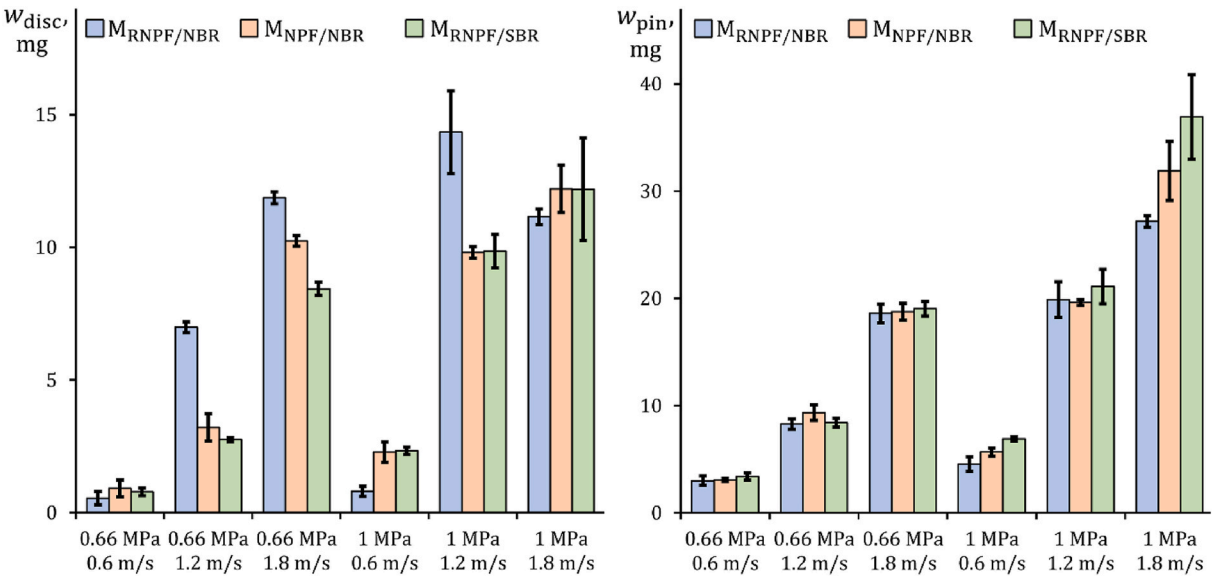

Fig. 6. Disc sample wear w_{disc} and pin sample wear w_{pin} depending on the friction regime.

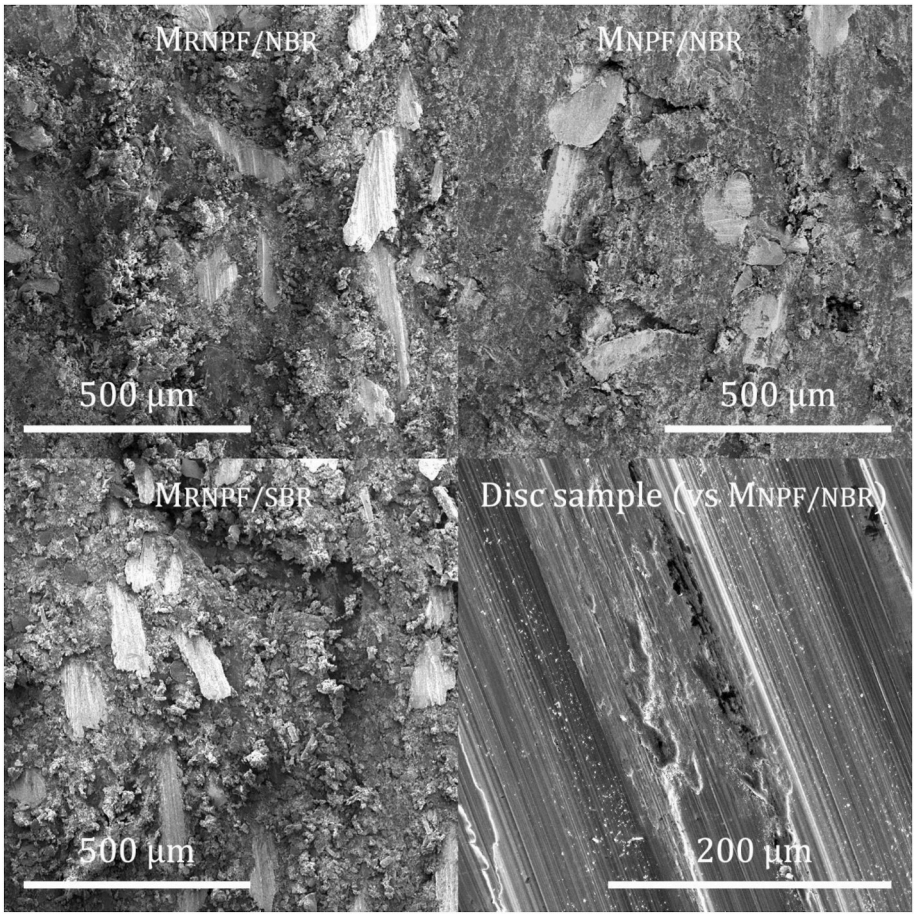

Fig. 7. SEM images of the worn surfaces of the pin and disc samples (1 MPa × 1.8 m/s).

relative wear with the change $M_{RNPF/NBR} \rightarrow M_{NPF/NBR}$ or $M_{RNPF/NBR} \rightarrow M_{RNPF/SBR}$ in the heavier FR. This trend is most probably related to the mechanical factor, specifically decrease in the hardness and strength properties of the pin sample (see Table 3). Jeganmohan et al. [23] reported a similar decrease in the brake disc wear when replacing NBR with SBR in the brake pad.

The dependencies of the pin sample wear w_{pin} (see Fig. 6) on the temperature T (see Fig. 5) and specific power P are shown in Fig. 14. The specific power P is calculated for each FR as the product of COF, contact pressure and sliding speed. On the one hand, the pronounced correlation w_{pin}-T for all FM and FR suggests a temperature sensitivity of the wear characteristics, which was previously reported for FM based on PF/NBR

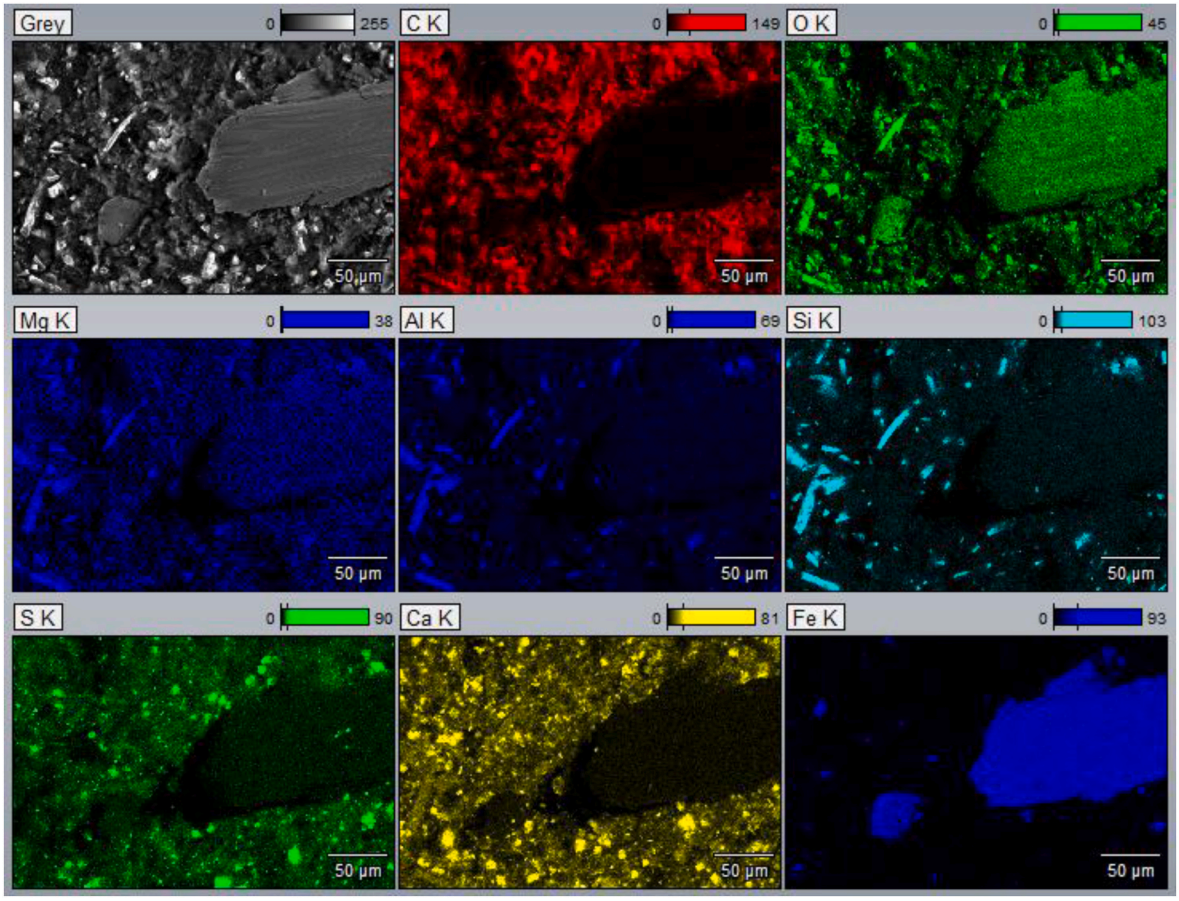

Fig. 8. EDX maps of the worn pin sample surface ($M_{RNPF/SBR}$, 1 MPa × 1.8 m/s).

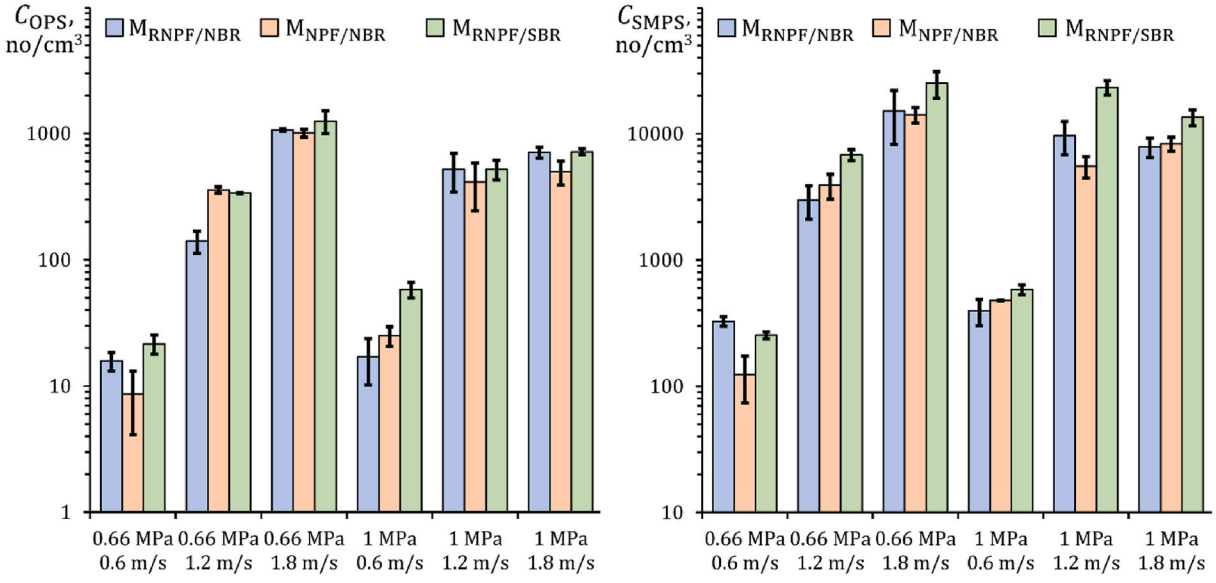

Fig. 9. Particle concentrations C_{OPS} and C_{SMPS} depending on the friction regime.

or PF/SBR by Liu et al. [26]. The possible cause-and-effect chain may thus have the following form: change of an ingredient in FM → changes in the thermal properties of FM (thermal conductivity, specific heat, density) → change in the temperature of FM → change in the integrity and strength properties of the binding mixture → change in the wear rate of FM. On the other hand, a significant scatter in w_{pin} at $P \approx 0.83$ W/mm^2, corresponding to the heaviest FR, allows hypothesising a direct dependence of the wear rate on the hardness and strength properties of the binding mixture which, in their turn, depend on the formulation of FM (Saffar and Shojaei [42]). In fact, the thermal and mechanical factors described are generally interrelated.

SEM/EDX analysis of the worn surfaces of the pin and disc samples

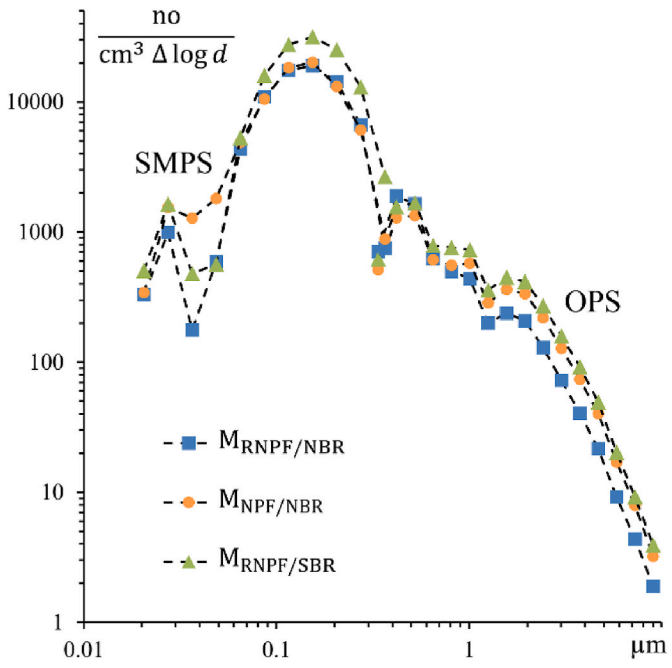

Fig. 10. Size distributions of airborne wear particles (1 MPa × 1.8 m/s).

(see Figs. 7 and 8) shows that the steel fibre in FM serves as the basis for forming the primary plateaus on the friction surface of the pin sample. The primary plateaus appear to carry the major fraction of the friction load from the disc sample, which is supported by the presence of the ploughing grooves on these plateaus and the friction surface of the disc sample. Comparison of the SEM/EDX maps of the worn friction surfaces to those of the original friction surfaces (see Fig. 1) allows concluding that the mineral fibres in FM retain their integrity and are not smeared over the friction surface.

Particle measurements (see Fig. 9) reveal that replacing NBR with SBR, i.e. $M_{RNPF/NBR} \rightarrow M_{RNPF/SBR}$, significantly intensifies the particle emission, whereas there is no distinct trend regarding the change $M_{RNPF/NBR} \rightarrow M_{NPF/NBR}$. This finding can be explained by the fact that the glass transition temperature of SBR ($\approx -40°C$) is lower than that of PF ($\approx 140°C$) and NBR ($\approx -20°C$) (Derakhshandeh et al. [47]). Accordingly, replacing NBR with SBR leads to a decrease in the glass transition temperature of the binding mixture. This was confirmed by Liu et al. [26] who reported that 'compared to the pure PF, the addition of SBR caused the glass transition temperature of the polymer matrix material to decrease from 150 °C to 136 °C'. Thereby, $M_{RNPF/SBR}$ is reasonably expected to have lower integrity and strength properties at elevated temperatures compared to $M_{RNPF/NBR}$.

The particle size distribution (see Fig. 10) exhibits peaks located at 0.15, 0.5 and 1.6 μm. Similar peaks were reported for train brake FM in several studies. For example, Namgung et al. [13], investigating non-asbestos organic metro train brake pads, found a peak at 0.2 μm (electric mobility) and another one at about 0.4 μm (optical diameter). Tsybrii et al. [14] reported an OPS distribution for a train brake lining material based on caoutchouc and PF exhibiting the same peak at 0.5 μm. The SEM images of the collected wear particles (see Fig. 11) show that the 1.6 μm order particles have flaky shape, as mentioned in Section 3. On the other hand, the smaller particles with size range covering 0.15 and 0.5 μm peaks are more rounded. As regards the agglomerated particles collected on the CI foils, they could have been formed at different stages: direct generation at the friction contact, clustering on the friction surface, clustering in the air, settling on the foil. The true evolution of an agglomerated particle can be hardly determined.

The EDX maps of the collected wear particles (see Fig. 12) indicate

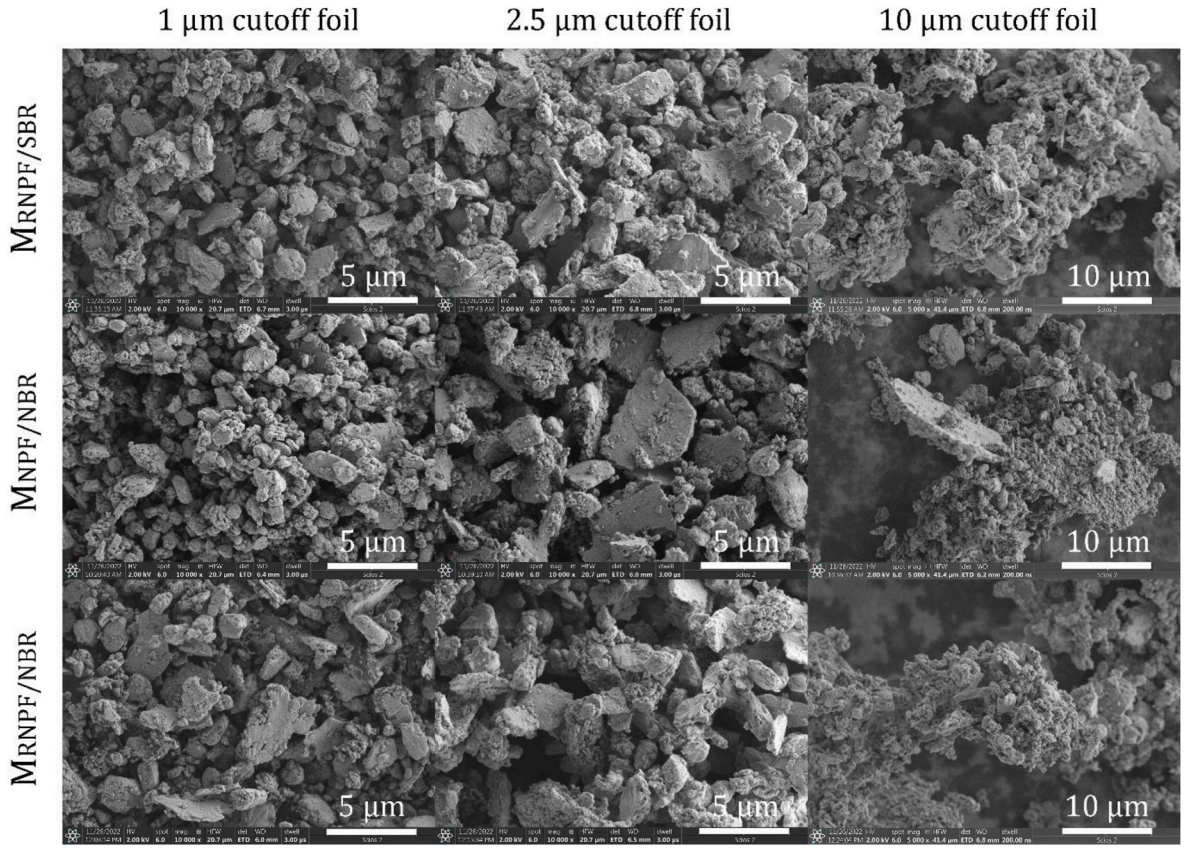

Fig. 11. SEM images of the collected wear particles.

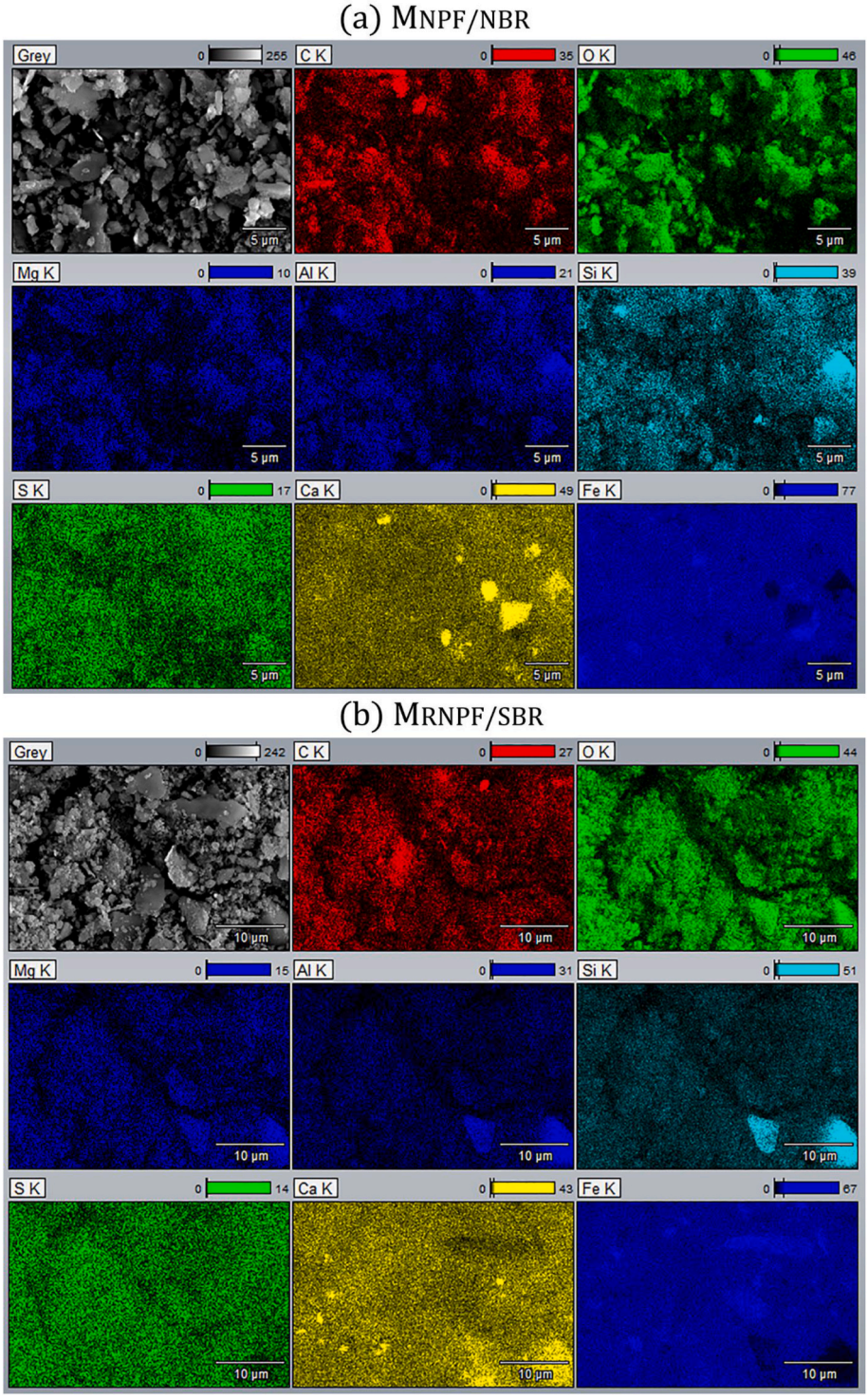

Fig. 12. EDX maps of the collected wear particles.

particles of different origin. The particles composed mainly of iron originate from wearing the steel disc sample and steel fibre in FM. Further, the micrometre-order particles with noticeable content of calcium (see Fig. 12a) originate from wearing calcium carbonate powder particles in FM. Furthermore, the particles containing silicon, aluminium, magnesium and oxygen originate from wearing the mineral fibre in FM. The size of such particles (see Fig. 12b) is approximately 5 µm which is comparable to the transverse size of the mineral fibres shown in Figs. 1 and 8. Fig. 15 compares the elemental composition of the collected wear particulate matter to that of FM (see Table 2), considering the elements whose content exceeds 2 wt%. Expectedly, the particles contain a large amount of iron as compared to FM. The iron content is about 50 wt% which agrees with the results obtained by Wahlström et al. [48] and Tsybrii et al. [14]. There are also noticeable contents of calcium and silicon which are close to those in FM. Note that silicon in the particles may also originate from wearing the disc sample (see Table 2). These results are confirmed for all foils with 1, 2.5 and 10 µm cut-off points.

The obtained experimental data allow analysing the wear mechanisms for the studied FM. It is known that at elevated temperatures, FM

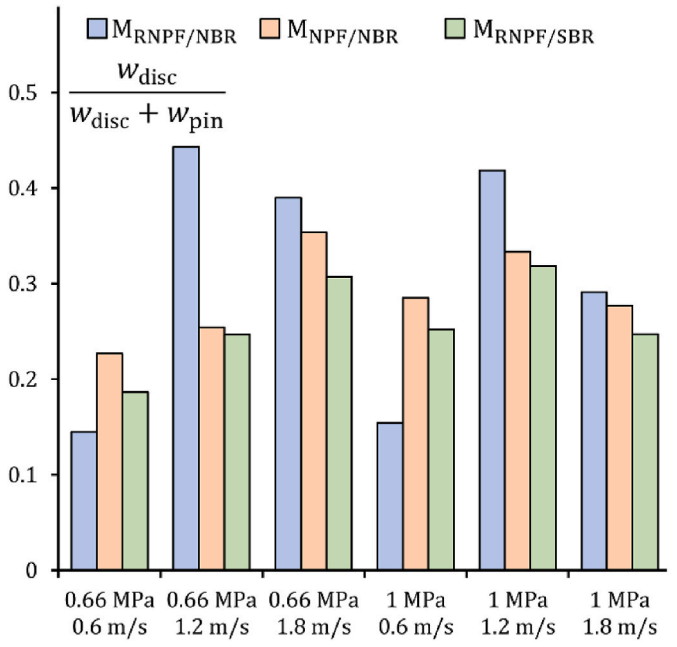

Fig. 13. Relative wear of the disc sample depending on the friction regime.

containing PF and/or rubber can emit vapours that interact with molecules of air, resulting in the nucleation of nanoparticles and their subsequent clustering. Namgung et al. [13] reported the emission of 10 nm order particles from a metro train brake dynamometer at temperatures above 70 °C. Nosko et al. [49] observed the emission of 1.3–10 nm particles from car brake FM at temperatures above 160 °C. Ma et al. [50] concluded that 5% of the ultrafine particles (below 0.1 μm) emitted from car brake FM at 200 °C are of non-friction nature. Relatively low concentrations of ultrafine particles observed in the present study (see Fig. 10) imply a negligible contribution of the nucleation mechanism of particle generation.

The friction-related generation of airborne particles (airborne wear particles) occurs due to different wear mechanisms including abrasion, adhesion and oxidation. The ploughing grooves on the primary plateaus and disc sample friction surface (see Fig. 7), as well as predominantly flaky shape of 1–10 μm wear particles (see Fig. 11), present strong pieces of evidence for the abrasive wear. Besides, the occurrence of wear particles (see Fig. 12b) that originate from the mineral fibres and are comparable to their transverse size implies that a single mineral fibre may not be gradually worn out but is fragmented into large pieces which are subsequently detached from the binding mixture and emitted in the form of wear particles. In a similar manner, a compact cluster of the calcium carbonate powder (see Fig. 12a) can be detached from the binding mixture. On the other hand, the collected submicron wear particles of rounded shape suggest a contribution of the adhesive mechanism (Olofsson [12]). There is lack of experimental data here to make stronger conclusions regarding this wear mechanism.

As mentioned by Kukutschová and Filip [1], friction and wear processes at temperatures above 300 °C are accompanied by oxidation of chemically unstable components, including PF and rubber, and associated emission of ultrafine particles. Low concentrations of ultrafine particles (see Fig. 10) and relatively low temperature of the pin sample (see Fig. 5) suggest that the contribution of the oxidative wear is negligibly small.

Summing up the obtained results, it has been shown that although the modification of NPF with resorcinol improves the hardness and strength properties of FM, this modification does not considerably affect the emission and properties of wear particles. Another practically important finding is that replacing SBR with NBR allows reducing the emission of 0.1–10 μm wear particles through increasing the glass transition temperature of the binding mixture. As mentioned in Section 2.5, the pin-on-disc tribomachine used in the present study simulates substantially milder friction conditions compared to those in train brakes. Therefore, these findings should undergo validation by brake dynamometer experiments.

5. Conclusions

The present study investigates the concentration, size distribution, morphology and elemental composition of airborne wear particles emitted from train brake friction materials (FM) with binding ingredients in the form of novolac phenol formaldehyde resin (NPF) or resorcinol-modified novolac phenol formaldehyde resin (RNPF) and nitrile butadiene rubber (NBR) or styrene butadiene rubber (SBR). The wear particles were generated under controlled conditions by a pin-on-disc tribomachine inside an aerodynamic chamber. They were counted, classified by size and collected using aerosol instruments based on the optical, electric mobility and aerodynamic measurement principles. The

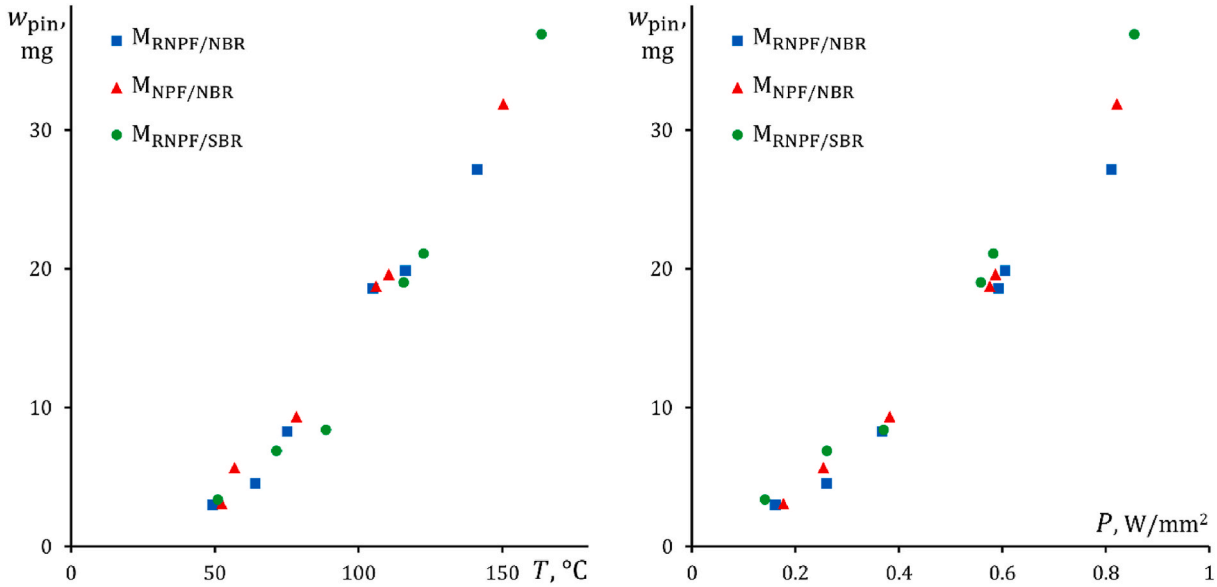

Fig. 14. Dependencies of the pin sample wear w_{pin} on the temperature T and specific power P.

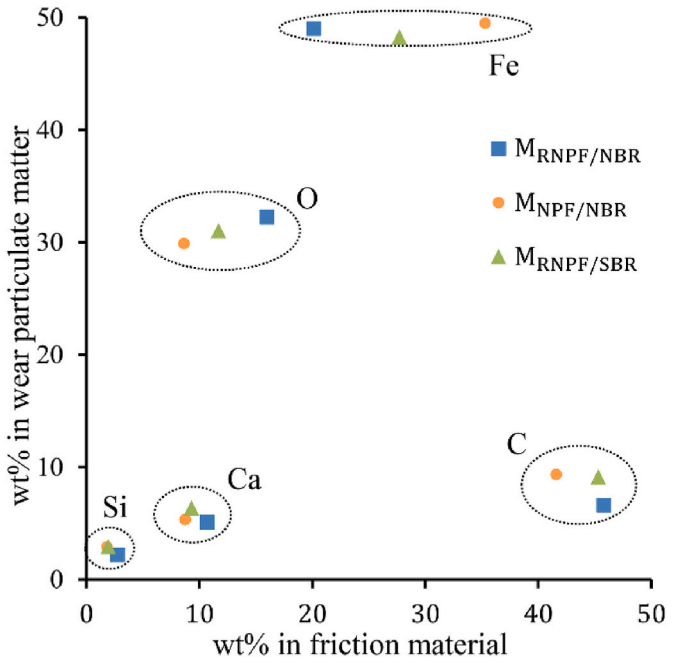

Fig. 15. Elemental compositions of the friction material and wear particulate matter collected on 1 μm cut-off foil.

morphology and elemental composition of the collected wear particles were studied using scanning electron microscopy and energy dispersive X-ray spectroscopy. The emission and properties of wear particles were analysed in relation to the mechanical properties of FM and wear mechanism.

The main findings can be summarised as follows:

- The replacement of 11.2 wt% NPF with RNPF in FM has no considerable effects on the emission and properties of wear particles. By contrast, replacing 11.2 wt% SBR with NBR in FM significantly reduces the emission of 0.1–10 μm wear particles, which is attributed to an increase in the glass transition temperature of the binding mixture and its higher integrity and strength properties at elevated temperatures.
- The particle size distribution exhibits peaks at 0.15, 0.5 and 1.6 μm. Wear particles in the order of 1.6 μm and larger have flaky shape and are generated via abrasive wear. On the other hand, smaller wear particles with size range covering 0.15 and 0.5 μm peaks are more rounded and are most probably generated via abrasive and adhesive wear.
- Most of the wear particles composed predominantly of iron originate from wearing the steel disc sample and steel fibre in FM. Fewer wear particles containing silicon, aluminium and magnesium originate from detaching large fragments of the mineral fibres from the binding mixture. Additionally, wear particles containing calcium originate from detaching compact clusters of the calcium carbonate powder from the binding mixture.

Funding

The present work was supported by the National Science Centre, Poland [grant number 2017/27/B/ST8/01249] and [grant number 2022/06/X/ST8/00167].

CRediT authorship contribution statement

Yurii Tsybrii: Writing – original draft, Supervision, Methodology, Investigation, Funding acquisition. **Oleksii Nosko:** Writing – review & editing, Methodology, Formal analysis, Conceptualization. **Izabela Zglobicka:** Writing – review & editing, Visualization, Investigation. **Michal Kuciej:** Writing – review & editing, Supervision, Resources.

Declaration of competing interest

The authors declare the following financial interests/personal relationships which may be considered as potential competing interests: Michal Kuciej reports financial support provided by the National Science Centre, Poland. Yurii Tsybrii reports financial support provided by the National Science Centre, Poland.

Data availability

No data was used for the research described in the article.

References

[1] J. Kukutschová, P. Filip, Review of brake wear emissions: a review of brake emission measurement studies: identification of gaps and future needs, in: F. Amato (Ed.), Non-exhaust Emissions, Academic Press, 2018, pp. 123–146, https://doi.org/10.1016/B978-0-12-811770-5.00006-6.
[2] E. Adamiec, Chemical fractionation and mobility of traffic-related elements in road environments, Environ. Geochem. Health 39 (2017) 1457–1468, https://doi.org/10.1007/s10653-017-9983-9.
[3] Y. Cheng, Y. Lin, C. Liu, Levels of PM10 and PM2.5 in Taipei rapid transit system, Atmos. Environ. 42 (31) (2008) 7242–7249, https://doi.org/10.1016/j.atmosenv.2008.07.011.
[4] E. Fridell, M. Ferm, A. Ekberg, Emissions of particulate matters from railways – emission factors and condition monitoring, Transport. Res. Transport Environ. 15 (4) (2010) 240–245, https://doi.org/10.1016/j.trd.2010.02.006.
[5] M. Gustafsson, G. Blomqvist, E. Swietlicki, A. Dahl, A. Gudmundsson, Inhalable railroad particles at ground level and subterranean stations – physical and chemical properties and relation to train traffic, Transport. Res. Transport Environ. 17 (3) (2012) 277–285, https://doi.org/10.1016/j.trd.2011.12.006.
[6] S. Abbasi, L. Olander, C. Larsson, U. Olofsson, A. Jansson, U. Sellgren, A field test study of airborne wear particles from a running regional train, Proc. Inst. Mech. Eng. F J. Rail Rapid Transit 226 (1) (2012) 95–109. https://doi:10.1177/0954409711408774.
[7] C. Colombi, S. Angius, V. Gianelle, M. Lazzarini, Particulate matter concentrations, physical characteristics and elemental composition in the Milan underground transport system, Atmos. Environ. 70 (2013) 166–178, https://doi.org/10.1016/j.atmosenv.2013.01.035.
[8] A. Cartenì, F. Cascetta, S. Campana, Underground and ground-level particulate matter concentrations in an Italian metro system, Atmos. Environ. 101 (2015) 328–337, https://doi.org/10.1016/j.atmosenv.2014.11.030.
[9] M. Cusack, N. Talbot, J. Ondráček, M.C. Minguillón, V. Martins, K. Klouda, J. Schwarz, V. Ždímal, Variability of aerosols and chemical composition of PM10, PM2.5 and PM1 on a platform of the Prague underground metro, Atmos. Environ. 118 (2015) 176–183, https://doi.org/10.1016/j.atmosenv.2015.08.013.
[10] Y. Cha, M. Tu, M. Elmgren, S. Silvergren, U. Olofsson, Variation in airborne particulate levels at a newly opened underground railway station, Aerosol Air Qual. Res. 19 (2019) 737–748, https://doi.org/10.4209/aaqr.2018.06.0225.
[11] H. Lee, Generation characteristics of the airborne wear particles emitted from the wheel–rail contact for various train velocities and their generation relation with the train velocity, Atmos. Environ. X 5 (2020) 100068, https://doi.org/10.1016/j.aeaoa.2020.100068.
[12] U. Olofsson, A study of airborne wear particles generated from the train traffic — block braking simulation in a pin-on-disc machine, Wear 271 (2011) 86–91, https://doi.org/10.1016/j.wear.2010.10.016.
[13] H.G. Namgung, J.B. Kim, M.S. Kim, M. Kim, S. Park, S.H. Woo, G.N. Bae, D. Park, S. B. Kwon, Size distribution analysis of airborne wear particles released by subway brake system, Wear 372–373 (2017) 169–176, https://doi.org/10.1016/j.wear.2016.12.026.
[14] Y. Tsybrii, I. Zglobicka, M. Kuciej, O. Nosko, K. Golak, Airborne wear particle emission from train brake friction materials with different contents of steel and copper fibres, Wear 504–505 (2022) 204424, https://doi.org/10.1016/j.wear.2022.204424.
[15] G. De Falco, G. Russo, S. Ferrara, V. De Soccio, A. D'Anna, Sustainable design of low-emission brake pads for railway vehicles: an experimental characterization, Atmos. Environ. X 18 (2023) 100215, https://doi.org/10.1016/j.aeaoa.2023.100215.
[16] J. Kukutschová, P. Moravec, V. Tomášek, V. Matějka, J. Smolík, J. Schwarz, J. Seidlerová, K. Šafářová, P. Filip, On airborne nano/micro-sized wear particles released from low-metallic automotive brakes, Environ. Pollut. 159 (4) (2011) 998–1006, https://doi.org/10.1016/j.envpol.2010.11.036.
[17] D.C. Jara, H. Jang, Synergistic effects of the ingredients of brake friction materials on friction and wear: a case study on phenolic resin and potassium titanate, Wear (2019) 430–431, https://doi.org/10.1016/j.wear.2019.05.011, 222–232.
[18] A.P.G. Nogueira, M. Leonardi, G. Straffelini, S. Gialanella, Sliding behavior and particle emissions of Cu-free friction materials with different contents of phenolic

resin, Tribol. Trans. 63 (2020) 770–779, https://doi.org/10.1080/10402004.2020.1753870.
[19] C.A. Pope, R.T. Burnett, M.J. Thun, E.E. Calle, D. Krewski, K. Ito, G.D. Thurston, Lung cancer, cardiopulmonary mortality, and long-term exposure to fine particulate air pollution, J. Am. Med. Assoc. 287 (2002) 1132–1141, https://doi.org/10.1001/jama.287.9.1132.
[20] H.L. Karlsson, L. Nilsson, L. Möller, Subway particles are more genotoxic than street particles and induce oxidative stress in cultured human lungs, Chem. Res. Toxicol. 18 (2005) 19–23, https://doi.org/10.1021/tx049723c.
[21] C. Bigert, M. Alderling, M. Svartengren, N. Plato, U. de Faire, P. Gustavsson, Blood markers of inflammation and coagulation and exposure to airborne particles in employees in the Stockholm underground, Occup. Environ. Med. 65 (2008) 655–658, https://doi.org/10.1136/oem.2007.038273.
[22] A. Borawski, Conventional and unconventional materials used in the production of brake pads – review, Sci. Eng. Compos. Mater. 27 (2020) 374–396, https://doi.org/10.1515/secm-2020-0041.
[23] S.R. Jeganmohan, D.G. Solomon, T.V. Christy, Effect of two different rubbers as secondary binders on the friction and wear characteristics of non-asbestos organic (NAO) brake friction materials, Tribol. Mater. Surface Interfac. 12 (2018) 71–84, https://doi.org/10.1080/17515831.2018.1449349.
[24] F.F. Binda, V.A. Oliveira, C.A. Fortulan, L.B. Palhares, C.G. Santos, Friction elements based on phenolic resin and slate powder, J. Mater. Res. Technol. 9 (2020) 3378–3383, https://doi.org/10.1016/j.jmrt.2020.01.032.
[25] K. Tang, A. Zhang, T. Ge, X. Liu, X. Tang, Y. Li, Research progress on modification of phenolic resin, Mater. Today Commun. 26 (2021) 101879, https://doi.org/10.1016/j.mtcomm.2020.101879.
[26] X.J. Liu, H.Q. Wang, X.Y. Wu, J. Bu, P.H. Cong, Effect of the rubber components on the mechanical properties and braking performance of organic friction materials, J. Macromol. Sci., Part B 53 (2014) 707–720, https://doi.org/10.1080/00222348.2013.857554.
[27] C. Menapace, M. Leonardi, M. Secchi, A. Bonfanti, S. Gialanella, G. Straffelini, Thermal behavior of a phenolic resin for brake pad manufacturing, J. Therm. Anal. Calorim. 137 (2019) 759–766, https://doi.org/10.1007/s10973-019-08004-2.
[28] I.M. Fareez, A.H. Jasni, M.N.F. Norrrahim, Nanofibrillated cellulose based bio-phenolic composites, in: M. Jawaid, M. Asim (Eds.), Phenolic Polymers Based Composite Materials, Springer, 2021, pp. 139–151, https://doi.org/10.1007/978-981-15-8932-4_9.
[29] A. Shojaei, M. Fahimian, B. Derakhshandeh, Thermally conductive rubber-based composite friction materials for railroad brakes – thermal conduction characteristics, Compos. Sci. Technol. 67 (13) (2007) 2665–2674, https://doi.org/10.1016/j.compscitech.2007.03.009.
[30] P. Wasilewski, Experimental study on the effect of formulation modification on the properties of organic composite railway brake shoe, Wear 390–391 (2017) 283–294, https://doi.org/10.1016/j.wear.2017.08.007.
[31] W. Sawczuk, A. Merkisz-Guranowska, D. Ulbrich, J. Kowalczyk, A.-M.R. Cañás, Investigation and modelling of the weight wear of friction pads of a railway disc brake, Materials 15 (2022) 6312, https://doi.org/10.3390/ma15186312.
[32] B.S. Joo, D.C. Jara, H.J. Seo, H. Jang, Influences of the average molecular weight of phenolic resin and potassium titanate morphology on particulate emissions from brake linings, Wear 450–451 (2020), https://doi.org/10.1016/j.wear.2020.203243, 203243.
[33] J.W. Gooch, Encyclopedic Dictionary of Polymers, Springer, 2011, p. 626.
[34] T. Ge, K. Tang, X. Tang, Preparation and properties of acetoacetic ester-terminated polyether pre-synthesis modified phenolic foam, Materials 12 (2019) 334, https://doi.org/10.3390/ma12030334.
[35] A.M. Motawie, E.M. Sadek, Adhesives and coatings from phenol-formaldehyde/resorcinol-formaldehyde resins, Polym. Adv. Technol. 9 (1998) 837–843.
[36] P. Gurunath, J. Bijwe, Potential exploration of novel green resins as binders for NAO friction composites in severe operating conditions, Wear 267 (2009) 789–796, https://doi.org/10.1016/j.wear.2009.02.012.
[37] K. Akshay, M. Arjun, S. Govind, V. Hrithwik, S. Akhil, N. Rahulan, Mechanical behavior of silicon carbide filled SBR/NBR blends, Mater. Today: Proc. 42 (2021) 1432–1436, https://doi.org/10.1016/j.matpr.2021.01.234.
[38] Y. Liu, Z. Fan, H. Ma, Y. Tan, J. Qiao, Application of nano powdered rubber in friction materials, Wear 261 (2006) 225–229, https://doi.org/10.1016/j.wear.2005.10.011.
[39] E. Surojo, D. Ariawan, R. Arsada, N. Muhayat, W.W. Raharjo, D.F. Smaradhana, Effect of nitrile butadiene rubber (NBR) on mechanical and tribological properties of composite friction brakes, Tribol. Indust. 41 (2019) 516–525, https://doi.org/10.24874/ti.2019.41.04.05.
[40] N. Bijwe, J. Bijwe, NBR-modified resin in fade and recovery module in non-asbestos organic (NAO) friction materials, Tribol. Lett. 27 (2007) 189–196, https://doi.org/10.1007/s11249-007-9225-x.
[41] A. Tamayo, F. Rubio, R. Pérez-Aparicio, L. Saiz-Rodríguez, J. Rubio, Preparation and properties of sustainable brake pads with recycled end-of-life tire rubber particles, Polymers 13 (2021) 3371, https://doi.org/10.3390/polym13193371.
[42] A. Saffar, A. Shojaei, Effect of rubber component on the performance of brake friction materials, Wear 274–275 (2012) 286–297, https://doi.org/10.1016/j.wear.2011.09.012.
[43] I. Mutlu, I. Sugözü, A. Keskin, The effects of porosity in friction performance of brake pad using waste tire dust, Polímeros 25 (5) (2015) 440–446, https://doi.org/10.1590/0104-1428.1860.
[44] B.S. Joo, Y.H. Chang, H.J. Seo, H. Jang, Effects of binder resin on tribological properties and particle emission of brake linings, Wear 434–435 (2019), https://doi.org/10.1016/j.wear.2019.202995, 202995.
[45] W. Song, J. Park, H. Seo, J. Choi, J.J. Lee, S.S. Sohn, H. Jang, Reduction of brake emission by optimizing the curing condition for brake pads using an artificial neural network, Wear 516–517 (2023), https://doi.org/10.1016/j.wear.2022.204606, 204606.
[46] W.J. Wang, F. Wang, K.K. Gu, H.H. Ding, H.Y. Wang, J. Guo, Q.Y. Liu, M.H. Zhu, Investigation on braking tribological properties of metro brake shoe materials, Wear 330–331 (2015), https://doi.org/10.1016/j.wear.2015.01.057, 498–506.
[47] B. Derakhshandeh, A. Shojaei, M. Faghihi, Effects of rubber curing ingredients and phenolic-resin on mechanical, thermal, and morphological characteristics of rubber/phenolic-resin blends, J. Appl. Polym. Sci. 108 (2008) 3808–3821, https://doi.org/10.1002/app.28034.
[48] J. Wahlström, L. Olander, U. Olofsson, Size, shape, and elemental composition of airborne wear particles from disc brake materials, Tribol. Lett. 38 (2010) 15–24, https://doi.org/10.1007/s11249-009-9564-x.
[49] O. Nosko, J. Vanhanen, U. Olofsson, Emission of 1.3–10 nm airborne particles from brake materials, Aerosol. Sci. Technol. 51 (1) (2017) 91–96, https://doi.org/10.1080/02786826.2016.1255713.
[50] J. Ma, U. Olofsson, Y. Lyu, J. Wahlström, A. Hedlund Åström, M. Tu, A comparison of airborne particles generated from disk brake contacts: induction versus frictional heating, Tribol. Lett. 68 (2020) 38, https://doi.org/10.1007/s11249-020-1279-z.